NASA/TM—2001-210822

Implementation of Fiber Substructuring Into Strain Rate Dependent Micromechanics Analysis of Polymer Matrix Composites

Robert K. Goldberg
Glenn Research Center, Cleveland, Ohio

April 2001

The NASA STI Program Office . . . in Profile

Since its founding, NASA has been dedicated to the advancement of aeronautics and space science. The NASA Scientific and Technical Information (STI) Program Office plays a key part in helping NASA maintain this important role.

The NASA STI Program Office is operated by Langley Research Center, the Lead Center for NASA's scientific and technical information. The NASA STI Program Office provides access to the NASA STI Database, the largest collection of aeronautical and space science STI in the world. The Program Office is also NASA's institutional mechanism for disseminating the results of its research and development activities. These results are published by NASA in the NASA STI Report Series, which includes the following report types:

- TECHNICAL PUBLICATION. Reports of completed research or a major significant phase of research that present the results of NASA programs and include extensive data or theoretical analysis. Includes compilations of significant scientific and technical data and information deemed to be of continuing reference value. NASA's counterpart of peer-reviewed formal professional papers but has less stringent limitations on manuscript length and extent of graphic presentations.

- TECHNICAL MEMORANDUM. Scientific and technical findings that are preliminary or of specialized interest, e.g., quick release reports, working papers, and bibliographies that contain minimal annotation. Does not contain extensive analysis.

- CONTRACTOR REPORT. Scientific and technical findings by NASA-sponsored contractors and grantees.

- CONFERENCE PUBLICATION. Collected papers from scientific and technical conferences, symposia, seminars, or other meetings sponsored or cosponsored by NASA.

- SPECIAL PUBLICATION. Scientific, technical, or historical information from NASA programs, projects, and missions, often concerned with subjects having substantial public interest.

- TECHNICAL TRANSLATION. English-language translations of foreign scientific and technical material pertinent to NASA's mission.

Specialized services that complement the STI Program Office's diverse offerings include creating custom thesauri, building customized data bases, organizing and publishing research results . . . even providing videos.

For more information about the NASA STI Program Office, see the following:

- Access the NASA STI Program Home Page at ***http://www.sti.nasa.gov***

- E-mail your question via the Internet to help@sti.nasa.gov

- Fax your question to the NASA Access Help Desk at 301–621–0134

- Telephone the NASA Access Help Desk at 301–621–0390

- Write to:
  NASA Access Help Desk
  NASA Center for AeroSpace Information
  7121 Standard Drive
  Hanover, MD 21076

NASA/TM—2001-210822

Implementation of Fiber Substructuring Into Strain Rate Dependent Micromechanics Analysis of Polymer Matrix Composites

Robert K. Goldberg
Glenn Research Center, Cleveland, Ohio

National Aeronautics and
Space Administration

Glenn Research Center

April 2001

Acknowledgments

The author would like to acknowledge Fiberite, Inc. for providing the material used for the experimental tests on the IM7/977–2 system along with additional information and data. The author would also like to acknowledge Prof. Amos Gilat of Ohio State University for conducting the tensile tests on the IM7/977–2 material presented in this report.

Available from

NASA Center for Aerospace Information
7121 Standard Drive
Hanover, MD 21076
Price Code: A03

National Technical Information Service
5285 Port Royal Road
Springfield, VA 22100
Price Code: A03

Available electronically at http://gltrs.grc.nasa.gov/GLTRS

IMPLEMENTATION OF FIBER SUBSTRUCTURING INTO STRAIN RATE DEPENDENT MICROMECHANICS ANALYSIS OF POLYMER MATRIX COMPOSITES

Robert K. Goldberg
National Aeronautics and Space Administration
Glenn Research Center
Cleveland, Ohio 44135

SUMMARY

A research program is in progress to develop strain rate dependent deformation and failure models for the analysis of polymer matrix composites subject to impact loads. Previously, strain rate dependent inelastic constitutive equations developed to model the polymer matrix were incorporated into a mechanics of materials based micromechanics method. In the current work, the micromechanics method is revised such that the composite unit cell is divided into a number of slices. Micromechanics equations are then developed for each slice, with laminate theory applied to determine the elastic properties, effective stresses and effective inelastic strains for the unit cell. Verification studies are conducted using two representative polymer matrix composites with a nonlinear, strain rate dependent deformation response. The computed results compare well to experimentally obtained values.

LIST OF SYMBOLS

A_{ij}	laminate stiffness matrix components
A_f^i	area of fiber portion of slice “i”
D_o	inelastic material constant representing maximum inelastic strain rate
d_f	fiber diameter
e	collected inelastic strain terms in solving for effective inelastic strains
h_f^i	thickness ratio of slice “i”
h_k	thickness of ply k in laminate
J_2	second invariant of deviatoric stress tensor
K_2	second invariant of deviatoric overstress tensor
N_{div}	number of fiber slices in composite unit cell
N_f	number of fiber slices in analysis cell
N_{ij}	total effective force resultant components for laminate
N_{ij}^I	components of force resultants due to inelastic strains for laminate
N_l	number of plies in laminate
n	inelastic material constant representing rate dependence of material
p_n	variable to be integrated in Runge-Kutta integration algorithm
Q_{ij}	plane stress stiffness matrix components for slice in material axis system
Q_{ijl}	plane stress stiffness matrix components for lamina in material axis system
$\overline{Q}_{ij}$	stiffness matrix components for lamina in structural axis system
q	inelastic material constant representing hardening rate of material
S_{ij}	compliance matrix components
S_{ijl}	compliance matrix components for lamina
s_{ij}	deviatoric stress components

t current time

Δt time increment

t_f thickness of fiber slice in unit cell

V_f fiber volume ratio of the composite or of the composite slice

y_i y-coordinate of top of slice "i" in analysis cell

Z_o material constant representing initial isotropic hardness of material

α scaling factor for shear components of K_2 effective stress

β material constant used in scaling shear components of K_2 effective stress

ε_{ij} strain tensor components

ε_{ij}^I inelastic strain components

ε_{ij}^o midplane strain components for laminate

ε_e^I effective inelastic strain

ε^I uniaxial inelastic strain in constant strain rate tensile test

$\dot{\varepsilon}_o$ total applied strain rate in constant strain rate uniaxial tensile test

ε_s^I inelastic strain at saturation in constant strain rate uniaxial tensile test

γ_{ij} engineering shear strain components

γ_{ij}^o midplane engineering shear strain components for laminate

θ fiber orientation angle for each ply in laminate

Ω_{ij} internal stress component

Ω uniaxial internal stress in constant strain rate tensile test

Ω_m inelastic material constant representing value of internal stress at saturation

σ_{ij} stress tensor components for slice and subslice

σ_{ijl} stress tensor components for lamina

σ uniaxial stress in constant strain rate tensile test

σ_s saturation stress in constant strain rate uniaxial tensile test

σ_m mean or hydrostatic stress

• quantities with dots above them represent rates with respect to time

Subscripts:

c stress and strain components for analysis cell
f fiber related material property
m matrix related material property
12 in-plane shear stress or strain components in material axis system
11,22 normal in-plane stress or strain components in material axis system
33 normal out-of-plane stress or strain components in material axis system
x,y normal in-plane stress or strain components in structural axis system
xy in-plane shear stress or strain components in structural axis systems

INTRODUCTION

NASA Glenn Research Center has an ongoing research program to investigate the feasibility of developing jet engine fan containment systems composed of polymer matrix composite materials. To design such a system, the ability to correctly predict the deformation and failure behavior of the composite under high rate loading conditions is required. Specifically, the analysis method must have the ability to account for any strain rate dependence and nonlinearities that might be present in the deformation response.

In previous research (ref. 1), an inelastic constitutive model has been developed to predict the nonlinear, rate dependent deformation response of ductile polymers. The equations have been implemented into a mechanics of materials based micromechanics model to enable the prediction of the nonlinear, rate dependent deformation response of carbon fiber reinforced polymer matrix composites. Classical lamination theory has also been implemented within the composite micromechanics (ref. 2) to allow for the analysis of symmetric thin laminates subject to in-plane loading.

In the original micromechanics, the composite unit cell was subdivided into four subcells, with one subcell composed of fiber material and the remaining three subcells representing the matrix. Uniform stress and uniform strain assumptions were applied to the unit cell to obtain the local and effective stress and strain values. This approach was similar to that taken by Sun and Chen (ref. 3), Robertson and Mall (ref. 4), and Pecknold and Rahman (ref. 5).

Several efforts have been made to develop more refined versions of this micromechanics approach. By utilizing a unit cell with a greater number of subcells, presumably more accurate results could be obtained. Pindera and Bednarcyk (ref. 6) developed a reformulated version of the Generalized Method of Cells (ref. 7), where the unit cell could be divided up into an arbitrary number of subcells. Uniform stress and uniform strain assumptions were still applied to the entire unit cell to obtain the local and effective stress and strain values. However, since the equations for each of the subcells were coupled to the equations for all the remaining subcells, fairly large systems of equations were obtained which needed to be solved. Whitney (ref. 8) divided the unit cell into a number of slices through the thickness. Uniform stress and uniform strain assumptions were then applied between the fiber and matrix within each slice to obtain the effective elastic constants for each slice. Effective elastic constants for the overall composite were then computed by averaging through the thickness. A similar approach was used by Greszczuk (ref. 9) to obtain the effective elastic constants of a composite and the interfiber stresses. By using a slicing approach, the equations for each slice were uncoupled, leading to smaller systems of equations. However, in these analyses the composites were assumed to have a linear elastic, rate independent deformation response.

Mital, Murthy and Chamis (ref. 10) used a slicing approach to compute the effective elastic constants and microstresses (fiber and matrix stresses) in ceramic matrix composites. In this work, a mechanics of materials approach was used to compute the effective elastic constants and microstresses in each slice of the unit cell. Laminate theory was then applied to obtain the effective elastic constants for the unit cell. Laminate theory was also used to compute the effective stresses in each slice, which was used to compute the microstresses. However, in this model Poisson effects were neglected in the micromechanics, and the analyses again assumed linear elastic, rate independent deformation.

In the present work, the micromechanics method developed in reference 1 is refined in order to apply the slicing approach developed in reference 10. The unit cell is divided up into a number of slices, and uniform stress and uniform strain assumptions are then applied to obtain the constituent and effective stresses for each slice, along with the effective inelastic strains for each slice. Laminate theory (ref. 2) is then applied to obtain the effective stresses, elastic constants, and effective inelastic strains for the lamina. By an additional application of the laminate theory, the effective total force resultants and force resultants due to inelastic strains for a symmetric, multilayered laminate can be computed. By applying this revised approach, the unit cell can be refined to a much greater degree while keeping the size of the system of equations that need to be solved relatively small.

In this paper, first a review of the inelastic constitutive model used to compute the rate dependent, inelastic deformation response of the polymer matrix is presented. Next, the revised micromechanics equations are developed. Additionally, the laminate theory that includes force resultants due to inelastic strains is reviewed. The numerical algorithms used to compute the deformation response of the composite are discussed. Finally, verification studies conducted using two representative polymer matrix composite systems are presented.

BACKGROUND

Polymer Constitutive Equations Overview

The Ramaswamy-Stouffer state variable constitutive equations (ref. 11), which were originally developed to analyze the viscoplastic deformation of metals above one-half of the melting temperature, have been modified to analyze the rate dependent, nonlinear deformation response of ductile polymers. There is some physical motivation in utilizing constitutive equations that were developed for viscoplastic metals to analyze the deformation response of

ductile polymers. For example, Ward (ref. 12) defined the "yield stress" in polymers identically to how researchers (ref. 11) have defined the "saturation stress" in metals. Specifically, the respective terms are used to define the stress level in a uniaxial tensile test where the stress-strain curve becomes flat and the inelastic strain rate equals the total strain rate. Polymers have been modeled previously using viscoplastic equations by authors such as Valisetty and Teply (ref. 13), Zhang and Moore (ref. 14), who modified Bodner's viscoplastic model (ref. 15), and Bordonaro (ref. 16), who modified Krempl's Viscoplasticity Theory Based on Overstress (ref. 17).

In state variable constitutive equations, a single unified strain variable is defined to represent all inelastic strains (ref. 11). Furthermore, in the state variable approach there is no defined yield stress. Inelastic strains are assumed to be present at all values of stress, only at a very small level in the "elastic" range of deformation. State variables, which evolve with stress and inelastic strain, are defined to represent the average effects of the deformation mechanisms.

Several limitations and assumptions have been specified in the development of the constitutive equations. Small strain conditions are assumed and temperature effects are neglected. The nonlinear strain recovery observed in polymers on unloading is not simulated, and phenomena such as creep, relaxation and high cycle fatigue are not accounted for in the equations. The equations are likely only to be valid for ductile polymers.

Polymer Flow and Evolution Equations

In the modified Ramaswamy-Stouffer model, the inelastic strain rate $\dot{\varepsilon}_{ij}^{I}$ is defined as a function of the deviatoric stress s_{ij} and a tensorial internal stress state variable Ω_{ij} (defined to have the properties of a deviatoric stress) in the form

$$\dot{\varepsilon}_{ij}^{I} = D_o \exp\left[-\frac{1}{2}\left(\frac{Z_o^2}{3K_2}\right)^n\right]\frac{s_{ij}-\Omega_{ij}}{\sqrt{K_2}} \tag{1}$$

where D_o, Z_o and n are material constants. The term K_2 is defined as

$$K_2 = \frac{1}{2}\left(s_{ij}-\Omega_{ij}\right)\left(s_{ij}-\Omega_{ij}\right) \tag{2}$$

and represents the second invariant of the overstress tensor. The elastic components of strain are added to the inelastic strain to obtain the total strain. The internal stress variable rate is defined by the equation

$$\dot{\Omega}_{ij} = \frac{2}{3}q\Omega_m\dot{\varepsilon}_{ij}^{I} - q\Omega_{ij}\dot{\varepsilon}_{e}^{I} \tag{3}$$

where q is a material constant, Ω_m is a material constant that represents the maximum value of the internal stress, and ε_e^I is the effective inelastic strain, defined in the normal manner used in inelastic analysis (ref. 11). The internal stress is assumed to be equal to zero when the material is in its virgin state.

The hydrostatic stress state has been found to have a significant effect on the yield behavior of a polymer (ref. 18). Bordonaro (ref. 16) indicated a possible way of accounting for such effects in a state variable constitutive model was to modify the effective stress terms. In this work, pressure dependence is included by multiplying the shear terms in the K_2 invariant in equation (2) by the correction factor

$$\alpha = \left(\frac{\sigma_m}{\sqrt{J_2}}\right)^{\beta} \tag{4}$$

where σ_m is the mean stress, J_2 is the second invariant of the deviatoric stress tensor, and β is a material constant.

The material constants that need to be determined include D_0, n, Z_0, Ω_m, q and β. The values of D_0, n, Z_0 and Ω_m required for equation (1) are characterized as follows. The value of D_0 is currently assumed to be equal to a value of 10^4 times the maximum applied strain rate, which correlates with the maximum inelastic strain rate. Equation (1) is simplified into its uniaxial form to model the results of a constant strain rate uniaxial tensile test, leading to the following expression

$$\dot{\varepsilon}^I = \frac{2}{\sqrt{3}} D_0 \exp\left[-\frac{1}{2}\left(\frac{Z_0}{|\sigma - \Omega|} \right)^{2n} \right] \frac{\sigma - \Omega}{|\sigma - \Omega|} \tag{5}$$

where $\dot{\varepsilon}^I$ is the uniaxial inelastic strain rate, σ is the uniaxial stress, and Ω is the uniaxial internal stress. The additional term of $2/\sqrt{3}$ results from the fact that stress deviators were used and the internal stress was originally defined as a deviatoric stress. By this definition, s_{11} equals $(2/3)\sigma$, and Ω_{11} equals $(2/3)\Omega$.

Next, equation (5) is rearranged as follows

$$-2 \ln\left(\frac{\sqrt{3}\dot{\varepsilon}^I}{2D_0} \right) = \left(\frac{Z_0}{\sigma - \Omega} \right)^{2n} \tag{6}$$

and the natural logarithm of both sides of the resulting expression is taken. The values of the inelastic strain rate, stress, and state variable Ω at saturation are substituted into the resulting expression, resulting in the following equation

$$\ln\left[-2 \ln\left(\frac{\sqrt{3}\dot{\varepsilon}_0}{2D_0} \right) \right] = 2n \ln(Z_0) - 2n \ln(\sigma_s - \Omega_m) \tag{7}$$

where σ_s equals the saturation stress, $\dot{\varepsilon}_o$ is the constant applied total strain rate in a constant strain rate uniaxial tensile test, and the remaining terms are as defined earlier.

The required constants are determined from a set of tensile curves obtained from constant strain rate tests. Each curve in this set is obtained at a different constant strain rate. Data pairs of the total strain rate and saturation stress values from each curve are taken. Values for Ω_m are estimated for the material, with initial estimates ranging from 50 to 75 percent of the highest saturation stress found to work well. These estimates are similar to the values used for large-grain metals. For each strain rate, the data values are substituted into equation (7), and represent a point on a master curve. The number of points in the master curve equal the number of strain rates at which tensile tests were conducted. A least squares regression analysis is then performed on the master curve. As suggested by equation (7), the slope of the best-fit line is equal to $-2n$. The intercept of the best-fit line is equal to $2n(\ln(Z_o))$. The value for Ω_m is then adjusted until an optimal fit to the data is obtained.

To determine the value for q for equation (3), first the equation is converted into its uniaxial equivalent and integrated, resulting in the following relation

$$\Omega = \Omega_m - \Omega_m \exp(-q\varepsilon^I) \tag{8}$$

where Ω is once again the uniaxial value of the internal stress and ε^I is the uniaxial inelastic strain. The elimination of the 2/3 term seen in equation (3) results from defining the internal stress as having the properties of a deviatoric stress. At saturation, the value of the internal stress is assumed to approach the maximum value, resulting in the exponential term approaching zero. Assuming that saturation occurs when the following condition is satisfied

$$\exp(-q\varepsilon_s^I) = 0.01 \tag{9}$$

the equation is solved for q, where ε_s^I is the inelastic strain at saturation. If the inelastic strain at saturation is found to vary with strain rate, the parameter q is computed at each strain rate and regression techniques are utilized to determine an expression for the variation of q.

Next, the material constant β in equation (4) is characterized. Since only uniaxial data were available for the polymers which were considered in this study, the value of the parameter β has been determined empirically by fitting data from composites with shear dominated fiber orientation angles, such as $[\pm 45°]_s$. To define the constant based on polymer data alone, a combination of tensile, torsion, and combined tension/torsion tests would be required.

Further information on the determination of the material constants can be found in Stouffer and Dame (ref. 11) and Goldberg (ref. 1).

Composite Micromechanics Model Overview

Micromechanics techniques are used to predict the effective properties and deformation response of the individual plies in a composite laminate. Laminate theory is then used to compute the effective deformation response of the entire composite. In the micromechanics, the effective properties and response are computed based on the properties of the individual constituents. The unit cell, the smallest material unit for which the response can be considered to be representative of the entire composite ply, is defined to consist of a single fiber and its surrounding matrix. Due to symmetry, only one-quarter of the unit cell needs to be analyzed.

As mentioned earlier, in the micromechanics methods used in references 1 and 2, the portion of the unit cell that was analyzed was divided into four rectangular subcells, one for the fiber and three matrix subcells. The area of the fiber subcell was set equal to one-fourth of the total fiber area. The relationship between the cross-section of a composite ply in the material axis system, the unit cell, and the portion of the unit cell that was analyzed in the original micromechanics is shown in figure 1.

To compute the local and effective stresses in the unit cell, the total strains applied to the unit cell and the inelastic strains in each subcell were assumed to be known. Assumptions of uniform stress and uniform strain were then applied to the unit cell. For example, along the fiber direction, the strains in each subcell were assumed to be uniform, and the stresses combined using volume and stiffness averaging. Transverse to the fiber direction in the plane of the composite, the stresses in each row of the subcells of the unit cell were assumed to be uniform, and the strains in each row were combined using volume averaging. Likewise, between rows the strains were assumed to be uniform, and the stresses combined using volume averaging. Similar assumptions were applied for in-plane shear loading. By combining these assumptions with the constitutive equations for the fiber and matrix, a system of six coupled simultaneous equations resulted which was solved for the stresses in each subcell. The full set of equations is presented in references 1 and 2.

REVISED MICROMECHANICS MODEL

Overview

In order to obtain more accurate numerical results, the ability to refine the unit cell to allow for a larger number of subcells is desirable. However, by applying the approach used previously, solving a large number of simultaneous equations would be required to obtain the subcell stresses. The number of simultaneous equations would increase as the number of subcells increased.

However, if one considers the combination of laminate theory with the micromechanics, one can observe that in classical laminate theory the unit cell is assumed to be in a global state of plane stress (since each ply must be in a state of plane stress). By assuming that each column of subcells in the original micromechanics model has uniform stresses, one can conclude that each row of the unit cell must also be in a state of plane stress. While the out-of-plane normal stresses in each subcell might be nonzero, when combined by volume averaging the total out-of-plane normal stress in each row must be zero. If one defines each row of the unit cell to be a slice, with this assumption, the behavior of each slice of the unit cell model can be decoupled. By applying uniform stress and uniform strain assumptions to each slice of the unit cell model, subslice (subcells within a particular slice) and effective stresses for each slice can be obtained. The results for each slice of the model could then be combined to obtain the effective stresses for the entire unit cell. The significance of this approach is that the subslice stresses for each row can be determined independently, allowing for a significant reduction in the number of simultaneous equations that need to be solved. Furthermore, no matter how many slices are included in the model, the size of the system of equations for each slice remains constant. Therefore, instead of solving one large set of simultaneous equations, multiple small sets of equations can be solved, which is much more computationally efficient.

As discussed earlier, Mital, Murthy and Chamis (ref. 10) applied exactly this approach to the analysis of ceramic matrix composites. They divided up the unit cell into an arbitrary number of horizontal rectangular slices. The effective elastic constants and microstresses were computed for each slice, and then laminate theory was applied to obtain the effective elastic constants for the entire unit cell. A similar approach will be applied for this work. The major difference is that in reference 10 a simplified mechanics of materials approach was applied within each slice to obtain the elastic constants and microstresses. As a result, Poisson effects were only applied indirectly, and the deformation was assumed to be linear elastic. In the current work inelastic strains are included. Additionally, by

using uniform stress and uniform strain assumptions similar to those used in references 1 and 2 within each slice, Poisson effects are fully included. As compared to reference 10, a slightly different algorithm is applied to determine the geometry of each slice. In the slicing algorithm presented here, an interface between the fiber and matrix is not included. Furthermore, a different methodology from that used in reference 10 is used to ensure that the total area of the fiber in the slices equals the actual area of the circular fiber.

For this study, the composites are assumed to have a periodic, square fiber packing and a perfect interfacial bond. Small strain conditions are assumed, and temperature effects are neglected. The fibers are assumed to be transversely isotropic and linearly elastic. The fibers are also assumed to have a circular cross-section. The matrix is assumed to be isotropic, with a rate dependent, nonlinear deformation response computed using the constitutive equations described in the previous section.

The general procedure in conducting an analysis using this methodology is as follows, which is summarized in figure 2. The strains applied to the composite laminate are assumed to be known, along with the inelastic strains in each subslice. The in-plane strains in each ply in the structural (laminate) axis system are assumed to be equal to the composite strains by the assumptions of laminate theory. The lamina (ply) strains are then transformed into the material axis system for the ply. A schematic demonstrating the difference between the material axis system and the structural axis system is shown in figure 3. In the figure, a ply at an arbitrary fiber orientation angle θ is shown. The material axis system "1-2" is displayed, where the "1" direction is along the fibers. The global "X-Y" structural axis system is also displayed. All of the plies in the laminate are oriented at various angles related to the structural axis system.

The in-plane strains in each slice are assumed to be equal to the lamina strains in the material axis system. Given the total strains in each slice and the inelastic strains in each subslice, the stresses in each subslice are computed. Once the stresses in each subslice are determined, the effective stresses and effective inelastic strains for the slice are computed. With this information, the effective stresses and inelastic strains for the lamina can be determined using laminate theory. By once again applying laminate theory, the effective force resultants and force resultants due to inelastic strains can be calculated for the laminate. The details of all of the steps of this procedure will be described in the following sections.

Slicing Algorithm

In the revised micromechanics the unit cell is divided up into several rectangular horizontal slices. The portion of the unit cell that contains fiber and matrix is divided up into an odd number of slices of equal thickness. The remaining matrix areas on the top and bottom of the unit cell are contained in individual slices (fig. 4). In figure 4, as an example the unit cell is divided up into five (5) fiber slices, and the portion of the unit cell which is analyzed (analysis cell) is divided up into three (3) fiber slices. As mentioned before, only one-quarter of the unit cell needs to be analyzed due to symmetry considerations. Figure 5 shows the analysis cell geometry in greater detail for an example of three fiber slices through the thickness and specifies the x-y coordinate system used in the slicing algorithm. Note that this "x-y" coordinate system is not the structural axis system described in the previous section, but is more closely related to the material axis system. However, to simplify the notation, in this section only the coordinate system axes are labeled "x" and "y". For the purposes of this algorithm, the unit cell is assumed to measure one unit in length by one unit in height, and the analysis cell is assumed to measure 0.5 units in length by 0.5 units in height.

The number of slices for the fiber in the entire unit cell (N_{div}) is related to the number of fiber slices in the analysis cell (N_f) through the following relationship

$$N_{div} = 2N_f - 1 \tag{10}$$

where in figures 4 and 5 N_{div} equals five (5) and N_f equals three (3). Note that as shown in the figures, in the analysis cell the bottom slice has a thickness equal to half that of the other fiber slices due to symmetry considerations.

The diameter of the fiber (d_f) is related to the fiber volume fraction of the overall composite (V_f) through the following relationship

$$d_f = \sqrt{\frac{4V_f}{\pi}} \tag{11}$$

and the thickness of each fiber slice in the entire unit cell (t_f) is equal to the fiber diameter (d_f) divided by the number of fiber slices in the entire unit cell (N_{div}).

To determine the location of the top of the "i"th slice in the y-coordinate direction (y_i) in the analysis cell, the following procedure is used. For the top fiber slice, the value of y_i is set equal to the fiber radius. For the remaining slices, the y-coordinate of the top of the slice is computed using the following expression

$$y_i = \left(i - \frac{1}{2}\right) t_f \tag{12}$$

where the 1/2 term results from the fact that the bottom slice in the analysis cell is one-half as thick as the remaining fiber slices.

The next step is to compute the fiber volume ratio and the thickness ratio (the ratio of slice thickness to total analysis cell thickness) for each slice. An important goal in computing the fiber volume fraction of each slice is to ensure that the total fiber area in the analysis cell is equal to one-fourth of the area of the actual fiber (assuming the actual fiber has a circular shape). As part of this process, the actual circular cross-section of the fiber has to be converted into a set of rectangular cross-sections. Furthermore, each rectangular cross-section must have the same area as the equivalent curvilinear cross-section.

To carry out this process, the following procedure is followed. First, note that for a circular fiber the x-coordinate of any point on the outer circumference of the actual fiber can be computed using the standard geometric definition of the radius of a circle and applying equation (11)

$$x = \sqrt{\frac{V_f}{\pi} - y^2} \tag{13}$$

where the x-coordinate varies continuously along the circumference of the fiber. Given the y-coordinates of the top and bottom of each slice, the area of the portion of the fiber contained within each slice (A_f^i) can be computed by using the standard calculus procedures for computing the area under a curve. Since the x-coordinate varies continuously within each slice, the area of the fiber contained within each slice can be obtained by integrating the equation for the x-coordinate (eq. (13)) between the y coordinates of the top and bottom of slice "i"

$$A_f^i = \int_{y_{i-1}}^{y_i} \sqrt{\frac{V_f}{\pi} - y^2}\, dy \tag{14}$$

By carrying out the integration, the following expression results

$$A_f^i = 0.5\left[y\sqrt{\frac{V_f}{\pi} - y^2} + \frac{V_f}{\pi} \sin^{-1}\left(y\sqrt{\frac{\pi}{V_f}} \right) \right]_{y_{i-1}}^{y_i} \tag{15}$$

where the value computed at y_{i-1} is subtracted from the value computed at y_i. For the bottom slice, y_{i-1} is equal to zero. By computing the fiber area in each slice in this manner, the total fiber area in the analysis cell is kept equal to one-quarter of the area of the actual circular fiber. The width of the rectangular fiber subslice can be computed by dividing the fiber area within the slice by the slice thickness.

The fiber volume fraction of each slice composed of fiber and matrix is equal to the fiber area in each slice divided by the slice area (the slice thickness multiplied by 0.5, the assumed width of the total slice). The thickness ratio for each slice (the ratio of the slice thickness to the total slice thickness) composed of both fiber and matrix (h_f^i) is equal to the slice thickness divided by 0.5, the assumed total height of the analysis cell. The fiber volume fraction of the top slice consisting of matrix only is set equal to zero. The thickness ratio of the top slice is equal to one minus the sum of the thickness ratio of the remaining slices.

Slice Micromechanics Equations

Each slice of the analysis cell shown in figures 4 and 5 is analyzed separately. The responses of each slice are then combined using laminate theory to obtain the effective response of the corresponding lamina. As mentioned previously, the advantage of this type of approach is that in analyzing a unit cell with a relatively large number of slices, multiple sets of four simultaneous equations can be solved instead of one large set of equations. Details and coordinate systems used for the slice analysis are shown in figure 6. Most of the slices are assumed to have two subslices, one subslice composed of fiber material and one subslice composed of matrix material. The top slice is assumed to be composed of matrix material only. The micromechanics equations presented here are for those slices composed of both fiber and matrix material. The stresses in the slices composed of pure matrix can be computed using the matrix elastic properties and inelastic constitutive equations. The fibers are assumed to be transversely isotropic and linearly elastic, and the matrix is assumed to be isotropic, with a rate dependent, nonlinear deformation response computed using the constitutive equations described earlier.

The transversely isotropic compliance matrix is used to relate the local strains to the local stresses in the fiber and matrix using the following relations

$$\begin{Bmatrix} \varepsilon_{11} \\ \varepsilon_{22} \\ \varepsilon_{33} \end{Bmatrix} = \begin{bmatrix} S_{11} & S_{12} & S_{12} \\ S_{12} & S_{22} & S_{23} \\ S_{12} & S_{23} & S_{22} \end{bmatrix} \begin{Bmatrix} \sigma_{11} \\ \sigma_{22} \\ \sigma_{33} \end{Bmatrix} + \begin{Bmatrix} \varepsilon_{11}^{I} \\ \varepsilon_{22}^{I} \\ \varepsilon_{33}^{I} \end{Bmatrix} \tag{16}$$

$$\gamma_{12} = S_{66}\sigma_{12} + 2\varepsilon_{12}^{I} \tag{17}$$

where all of the stresses and strains are assigned in a Cartesian frame of reference. Note that engineering shear strains are used in the analysis. A superscript "*I*" is used to denote inelastic strains. In these equations S_{ij} represents the components of the compliance matrix, not the components of the deviatoric stress tensor s_{ij} as in the discussion of the constitutive equations. Transverse shear stresses are neglected in the current analysis. However, since these stresses might turn out to be significant in impact problems, they might be included in the future using methods similar to those discussed here. Out-of-plane normal stresses are included in the analysis since even though each slice is assumed to be in a state of global plane stress, the individual subslices of each slice are assumed to be a full three-dimensional state of stress.

The addition of the inelastic strain components to the standard transversely isotropic elastic constitutive law allows the incorporation of inelasticity into the constitutive relations. For the fiber, which is assumed to be linear elastic, these components are neglected. For the matrix material, which is assumed to be isotropic, S_{23} is set equal to S_{12} and S_{22} is set equal to S_{11}.

In the equations that follow, the subscript "*f*" will be used to denote fiber related properties, and the subscript "*m*" will be used to denote matrix related properties. Stresses and strains with no subscript will be used to represent effective stresses and strains for the slice (not the composite ply or laminate). The symbol "V_f" will be used in this section to represent the fiber volume ratio for the slice, computed using the methods discussed earlier, not the total fiber volume fraction for the composite.

Along the fiber direction (direction 1 in fig. 6), the strains are assumed to be uniform in each subslice, and the stresses are combined using volume averaging. The in-plane transverse normal stresses (2 direction) and the in-plane shear stresses (1-2 direction) are assumed to be uniform in each subslice, and the strains are combined using volume averaging. The out-of-plane strains (3 direction) are assumed to be uniform in each subslice. The volume average of the out-of-plane stresses in each subslice is assumed to be equal to zero, enforcing a plane stress condition on the global level for the slice. These assumptions can be expressed using the following equations, which can be derived using the slice geometry shown in figure 6, the definition of the slice fiber volume ratio and the basic definitions of displacement and force equilibrium

$$\varepsilon_{11f} = \varepsilon_{11m} = \varepsilon_{11} \tag{18}$$

$$\varepsilon_{22} = V_f\varepsilon_{22f} + (1 - V_f)\varepsilon_{22m} \tag{19}$$

$$\varepsilon_{33f} = \varepsilon_{33m} = \varepsilon_{33} \tag{20}$$

$$\gamma_{12} = V_f \gamma_{12f} + (1 - V_f)\gamma_{12m} \tag{21}$$

$$\sigma_{11} = V_f \sigma_{11f} + \left(1 - V_f\right)\sigma_{11m} \tag{22}$$

$$\sigma_{22} = \sigma_{22f} = \sigma_{22m} \tag{23}$$

$$\sigma_{33} = 0 = V_f \sigma_{33f} + \left(1 - V_f\right)\sigma_{33m} \tag{24}$$

$$\sigma_{12} = \sigma_{12f} = \sigma_{12m} \tag{25}$$

where the stresses and strains are for the slice only, not for the composite ply or for the laminate as a whole. These assumptions can be (and were in references 1 and 2) applied to the entire unit cell, but for this work are only applied to each slice.

By combining the uniform stress and uniform strain assumptions (eqs. (18) to (25)) with the constituent stress-strain relations (eqs. (16) and (17)), the following system of equations results

$$\varepsilon_{11} - \frac{S_{12f}}{S_{22f} + S_{11m}\left(\dfrac{V_f}{1 - V_f}\right)}\varepsilon_{33m}^{I} = \left[S_{11f} - \frac{S_{12f}^2}{S_{22f} + S_{11m}\left(\dfrac{V_f}{1 - V_f}\right)}\right]\sigma_{11f} + \left[\frac{S_{12f}S_{12m}}{S_{22f} + S_{11m}\left(\dfrac{V_f}{1 - V_f}\right)}\right]\sigma_{11m} + \left[S_{12f} + \frac{S_{12f}\left(S_{12m} - S_{23f}\right)}{S_{22f} + S_{11m}\left(\dfrac{V_f}{1 - V_f}\right)}\right]\sigma_{22} \tag{26}$$

$$\varepsilon_{11} - \varepsilon_{11m}^{I} + \left(\frac{V_f}{1 - V_f}\right)\frac{S_{12m}}{S_{22f} + S_{11m}\left(\dfrac{V_f}{1 - V_f}\right)}\varepsilon_{33m}^{I} = \frac{V_f}{1 - V_f}\left[\frac{S_{12f}S_{12m}}{S_{22f} + S_{11m}\left(\dfrac{V_f}{1 - V_f}\right)}\right]\sigma_{11f} + \left[S_{11m} - \left(\frac{V_f}{1 - V_f}\right)\frac{S_{12m}^2}{S_{22f} + S_{11m}\left(\dfrac{V_f}{1 - V_f}\right)}\right]\sigma_{11m} + \left[S_{12m} - \left(\frac{V_f}{1 - V_f}\right)\frac{S_{12m}\left(S_{12m} - S_{23f}\right)}{S_{22f} + S_{11m}\left(\dfrac{V_f}{1 - V_f}\right)}\right]\sigma_{22} \tag{27}$$

$$\varepsilon_{22} - \left(1 - V_f\right)\varepsilon_{22m}^{I} - \frac{V_f\left(S_{23f} - S_{12m}\right)}{S_{22f} + S_{11m}\left(\dfrac{V_f}{1 - V_f}\right)}\varepsilon_{33m}^{I} = V_f\left[S_{12f} - \frac{S_{12f}\left(S_{23f} - S_{12m}\right)}{S_{22f} + S_{11m}\left(\dfrac{V_f}{1 - V_f}\right)}\right]\sigma_{11f}$$

$$+\left[\left(1 - V_f\right)S_{12m} + \frac{V_f S_{12m}\left(S_{23f} - S_{12m}\right)}{S_{22f} + S_{11m}\left(\dfrac{V_f}{1 - V_f}\right)}\right]\sigma_{11m}$$

$$+\left[V_f S_{22f} + (1 - V_f)S_{11m} + V_f\left(S_{23f} - S_{12m}\right)\frac{S_{12m} - S_{23f}}{S_{22f} + S_{11m}\left(\dfrac{V_f}{1 - V_f}\right)}\right]\sigma_{22} \tag{28}$$

$$\gamma_{12} = [V_f S_{66f} + (1 - V_f)S_{66m}]\sigma_{12} + 2(1 - V_f)\varepsilon_{12m}^{I} \tag{29}$$

that can be solved for the unknown stresses in the subslices. Note that σ_{22} and σ_{12} in the subslices are equal to the equivalent slice stresses due to the uniform stress assumptions. The total strains and subslice inelastic strains are considered to be the known values in solving this problem. These equations correspond to block five (5) in the analysis process (fig. 2), where the subslice stresses are computed knowing the slice strains and subslice inelastic strains.

By substituting the subslice stresses back into equations (22) to (25), an expression relating the effective stresses to the effective strains in the slice is obtained

$$\begin{Bmatrix}\sigma_{11}\\ \sigma_{22}\\ \sigma_{12}\end{Bmatrix} = \begin{bmatrix}Q_{11} & Q_{12} & 0\\ Q_{21} & Q_{22} & 0\\ 0 & 0 & Q_{66}\end{bmatrix}\begin{Bmatrix}\varepsilon_{11}\\ \varepsilon_{22}\\ \gamma_{12}\end{Bmatrix} + \begin{Bmatrix}e_1\\ e_2\\ e_3\end{Bmatrix} \tag{30}$$

where $[Q_{ij}]$ represents the effective plane stress stiffness matrix for the slice and $\{e_i\}$ represents the collected inelastic strain terms resulting from the calculations. This equation is important in two respects. First, through the process of obtaining this equation the effective elastic constants for the slice are computed (the $[Q_{ij}]$ effective plane stress stiffness matrix). Second, this equation represents the first task in block six (6) in the analysis process (fig. 2), computing the effective stresses in the slice given the subslice stresses. Note that due to uniform stress assumptions, only σ_{11} for the slice is computed in the algorithm using this expression, since the other slice stresses were computed earlier. To complete the second task in block six (6), the computation of the effective inelastic strains in the slice, the $\{e_i\}$ vector is brought to the left hand side of equation (30) and the expression is again inverted. By comparing the result to the transversely isotropic constitutive relation for the slice (similar to eqs. (16) and (17) for the fiber and matrix), the effective inelastic strains for the slice can be computed using the following expression

$$\begin{Bmatrix}\varepsilon_{11}^{I}\\ \varepsilon_{22}^{I}\\ \gamma_{12}^{I}\end{Bmatrix} = \begin{bmatrix}S_{11} & S_{12} & 0\\ S_{21} & S_{22} & 0\\ 0 & 0 & S_{66}\end{bmatrix}\begin{Bmatrix}e_1\\ e_2\\ e_3\end{Bmatrix} \tag{31}$$

where $[S_{ij}]$ is the effective compliance matrix for the slice, and $\{\varepsilon_{ij}^{I}\}$ represents the effective inelastic strain vector for the slice.

Lamina Effective Stiffness Matrix and Effective Inelastic Strains

To compute the effective stiffness matrix and effective inelastic strains for the lamina (which is equivalent to the equivalent properties for the analysis cell) from the effective stiffness matrix and inelastic strains for each slice, the following procedure is used. First, the in-plane strains for each slice are assumed to be constant and equal to the in-plane strains for the lamina. The total in-plane stresses for the lamina are assumed to be equal to the volume average of the in-plane stresses for each slice, as follows

$$\begin{Bmatrix} \sigma_{11} \\ \sigma_{22} \\ \sigma_{12} \end{Bmatrix}_l = \sum_{i=1}^{N_f+1} \begin{pmatrix} \sigma_{11} \\ \sigma_{22} \\ \sigma_{12} \end{pmatrix}_i h_f^i \tag{32}$$

where N_f is the number of fiber slices in the analysis cell, $\{\sigma_{ij}\}_l$ are the effective stresses in the lamina, h_f^i represents the thickness ratio of each slice as defined earlier, and the summation is over all of the slices (i). This step also accomplishes the first goal of block seven (7) in the analysis process (fig. 2), computing the effective lamina stresses given the effective stresses in each slice.

To compute the plane stress stiffness matrix and effective inelastic strains for the lamina, equation (30) for the slice is rewritten as

$$\begin{Bmatrix} \sigma_{11} \\ \sigma_{22} \\ \sigma_{12} \end{Bmatrix} = \begin{bmatrix} Q_{11} & Q_{12} & 0 \\ Q_{21} & Q_{22} & 0 \\ 0 & 0 & Q_{66} \end{bmatrix} \begin{Bmatrix} \varepsilon_{11} - \varepsilon_{11}^I \\ \varepsilon_{22} - \varepsilon_{22}^I \\ \gamma_{12} - \gamma_{12}^I \end{Bmatrix} \tag{33}$$

where equation (31) is applied to compute the $\{\varepsilon_{ij}^I\}$ vector from the $\{e_i\}$ vector. By substituting equation (33) into equation (32), the effective plane stress stiffness matrix for the lamina $[Q_{jk}]_l$, required for future steps in the analysis, is obtained as follows

$$[Q_{jk}]_l = \sum_{i=1}^{N_f+1} [Q_{jk}]_i h_f^i \tag{34}$$

where the summation is again over all of the slices. Likewise, by following the same procedures used to go from equation (30) to equation (31), the following expression is obtained for computing the effective inelastic strains for the lamina

$$\begin{Bmatrix} \varepsilon_{11}^I \\ \varepsilon_{22}^I \\ \gamma_{12}^I \end{Bmatrix}_l = \begin{bmatrix} S_{11} & S_{12} & 0 \\ S_{21} & S_{22} & 0 \\ 0 & 0 & S_{66} \end{bmatrix}_l \sum_{i=1}^{N_f+1} \begin{bmatrix} Q_{11} & Q_{12} & 0 \\ Q_{21} & Q_{22} & 0 \\ 0 & 0 & Q_{66} \end{bmatrix}_i \begin{Bmatrix} \varepsilon_{11}^I \\ \varepsilon_{22}^I \\ \gamma_{12}^I \end{Bmatrix}_i h_f^i \tag{35}$$

where $\{\varepsilon_{ij}^I\}_l$ is the effective inelastic strain vector for the lamina and $[S_{ij}]_l$ is the effective compliance matrix for the lamina. The computing of the effective inelastic strains for the lamina also represents the second task of block seven (7) of the analysis process (fig. 2).

Basic Equations of Laminate Theory

To allow for the analysis of multilayered laminates, where each ply can have a unique fiber orientation, the micromechanics method described above is combined with classical lamination theory (ref. 19). As will be described below, the force resultants due to inelastic strains are computed in a manner similar to that used to determine thermal and moisture resultants in the classical theory. As has been the case throughout this report, small strain conditions are assumed, and thermal and moisture effects are neglected. The composites are assumed to be thin

laminates under plane stress and the effective out-of-plane stresses for each ply are assumed to be zero. Only symmetric laminates under in-plane loading conditions with no bending effects are analyzed. In the future, the ability to analyze unsymmetric laminates will be added to the theory. Furthermore, since in the analysis of impact problems the effects of transverse shear stresses could be significant, the ability to account for these stresses will be added to the laminate theory in the future.

In the laminate theory for symmetric laminates, the total laminate force resultants $\{N_i\}$ are related to the mid-plane laminate strains $\{\varepsilon_i^o\}$ and the laminate force resultants due to inelastic strains $\{N_i^I\}$ by the following expression

$$\begin{Bmatrix} N_x \\ N_y \\ N_s \end{Bmatrix} = \begin{bmatrix} A_{xx} & A_{xy} & A_{xs} \\ A_{xy} & A_{yy} & A_{ys} \\ A_{xs} & A_{ys} & A_{ss} \end{bmatrix} \begin{Bmatrix} \varepsilon_x^o \\ \varepsilon_y^o \\ \gamma_s^o \end{Bmatrix} - \begin{Bmatrix} N_x^I \\ N_y^I \\ N_s^I \end{Bmatrix} \tag{36}$$

where the stresses and strains are in the structural (laminate) axis system and $[A_{ij}]$ represents the effective in-plane stiffness matrix for the laminate. The laminate stiffness matrix is computed using the stiffness matrices for each ply using standard laminate theory procedures (refs. 2 and 19). The subscripts "x" and "y" represent normal quantities in the structural axis system and the subscript "*s*" represents in-plane shear quantities in the structural axis system. Recall that figure 3 shows the relationship between the structural axis system and the material axis system. As before, note that engineering shear strains are used in the analytical development. Equation (36) is also used to carry out block eight (8) of the analysis process (fig. (2)), the computation of effective force resultants for the laminate.

The following summation over all of the plies is used to compute the terms in the force resultants due to inelastic strains $\{N_i^I\}$

$$\begin{Bmatrix} N_x^I \\ N_y^I \\ N_s^I \end{Bmatrix} = \sum_{k=1}^{N_l} \left[\overline{Q}_{ij}\right]_k \begin{Bmatrix} \varepsilon_x^I \\ \varepsilon_y^I \\ \varepsilon_s^I \end{Bmatrix}_k h_k \tag{37}$$

where $[\overline{Q}_{ij}]$ represents the plane stress stiffness matrix $[Q_{ij}]_l$ transformed into the structural axis system for ply k, $\{\varepsilon_i^I\}$ represents the effective inelastic strain vector in the structural axis system for ply k, N_l represents the total number of plies in the laminate and h_k represents the thickness of each ply. The plane stress stiffness matrix for each ply is transformed from the material axis system to the structural axis system using standard laminate theory procedures (refs. 2 and 19). The computation of the force resultants due to inelastic strains for the laminate is part of block eight (8) of the analysis process (fig. 2).

NUMERICAL IMPLEMENTATION OF ANALYTICAL MODEL

To verify the analytical model, a stand-alone computer code has been developed. A standard fourth order Runge-Kutta explicit integration routine is used to integrate the rate equations in the polymer constitutive model (ref. 20). For this class of equations, implicit integration routines have often been used because of their inherent numerical stability (ref. 11). However, in this case, to facilitate the implementation of these equations into a transient dynamic finite element code, explicit methods have been used. The Runge-Kutta method has been used due to its simplicity and ease of implementation. However, in the future more sophisticated integration algorithms may be used.

To compute the value of a set of variables p_n at time step $t + \Delta t$, where t is the current time and Δt is the time increment, the following equations are used

$$p_n(t + \Delta t) = p_n(t) + \frac{1}{6}\left(k_1 + 2k_2 + 2k_3 + k_4\right) \tag{38}$$

$$k_1 = \dot{p}_n\left(t, p_n\right)\Delta t \tag{39}$$

$$k_2 = \dot{p}_n\left(t + \frac{1}{2}\Delta t, p_n + \frac{1}{2}k_1\right)\Delta t \tag{40}$$

$$k_3 = \dot{p}_n\left(t + \frac{1}{2}\Delta t, p_n + \frac{1}{2}k_2\right)\Delta t \tag{41}$$

$$k_4 = \dot{p}_n\left(t + \Delta t, p_n + k_3\right)\Delta t \tag{42}$$

where $\dot{p}_n$ is the time derivative of variable p_n.

In the stand-alone computer code, first the geometric data and material properties are read in from an input file. Next, the loading information is input. Both stress and strain controlled loading is permitted. The slice geometry is computed using the procedures described earlier (eqs. (10) to (15)). The elastic properties for each slice and for the lamina are determined next (eqs. (30) and (34), respectively). From this information, the laminate stiffness matrix is computed (based on eq. (36)).

For each load step, the total strain rates or stress rates in the loading directions are calculated. The Runge-Kutta integration routine is then carried out to determine the inelastic strains and internal stresses in each subslice in the laminate, as well as the midplane strains and force resultants due to inelastic strains for the laminate. The procedure for the Runge-Kutta integration is described below and is carried out four times for each time step as indicated by equations (38) to (42). The total force resultants for the laminate are computed using equation (36). If the laminate is assigned a total thickness of one (1), the force resultants are equal to the stresses. Appropriate values are written to an output file, and the code proceeds to the next time step.

Within the Runge-Kutta integration routine, the strains in each lamina are converted into the material axis system. Within each ply, the stresses in the subslices of each slice are computed (eqs. (26) to (29)). At this point, the polymer constitutive equations (eqs. (1) to (4)) are applied to calculate the inelastic strain rate and internal stress rate for each matrix subslice. Next, the effective inelastic strain rate for each ply is computed in the material axis system (using rate forms of eqs. (31) and (35)) and converted to the structural axis system.

The next step in the Runge-Kutta routine is to compute the laminate force resultant rate due to inelastic strains for the laminate (eq. (37) in rate form). From this information, the laminate strain rate in each coordinate direction is determined. This procedure varies depending on whether the loading is strain controlled or stress controlled. For strain controlled loading, a partial inversion of the rate form of equation (36) is carried out, while for stress controlled loading a full inversion of the rate form of equation (36) is required.

MODEL VALIDATION

To verify the micromechanics equations, a series of analyses have been carried out using two polymer matrix composite systems. Both material systems exhibit a strain rate dependent, nonlinear deformation response.

Material Properties

The first material examined, supplied by Fiberite, Inc., consists of carbon IM7 fibers in a 977–2 toughened epoxy matrix. Tensile tests have been conducted on the neat resin and composite laminates with fiber orientations of [45°], [90°], and $[\pm 45°]_s$. Tensile tests were conducted at Ohio State University. Tests were conducted at strain rates of about 5×10^{-5}/sec and about 1.0/sec. Dog-bone shaped specimens were used with a gage length of approximately 0.9525 cm. The testing was conducted using an Instron hydraulic testing machine. Further details of the test specimens and testing procedures will be described in a future report (ref. 21), along with a discussion of high strain rate tests that were conducted.

The IM7/977–2 composite has a fiber volume ratio of 0.60. The material properties used in this study for the IM7 fiber are listed in table I. The longitudinal modulus, longitudinal Poisson's ratio and in-plane shear modulus are as given in reference 22. The transverse modulus of the fiber was reduced slightly from the value given in

reference 22 in order to provide a good correlation in the elastic range with the [90°] data. Since the transverse modulus given in reference 22 was also a correlated value, a variation of this sort was considered acceptable. The value for the transverse Poisson's ratio was taken from reference 23 based on representative carbon fiber data.

The material properties for the 977–2 resin were determined using the procedures described earlier in this report from the experimental uniaxial stress-strain curves shown in figure 7. Note that since this resin did not reach a "saturation" stress before failure, appropriate values were extrapolated from the tensile data and used to obtain the material properties. The value for the constant "β" required for the correction factor given in equation (4) was determined to be strain rate dependent. In addition, the material constant "q" from equation (3) was found to be rate dependent for this material. The values of the material constants for the 977–2 resin are given in table II. Stress-strain curves computed using the material constants given in table II are shown in figure 7 along with the experimental values. As can be seen in the figure, there is a good correlation between the experimental and computed curves.

The second material system examined consists of carbon AS4 fibers embedded in a PEEK thermoplastic matrix. Tensile stress strain curves were obtained by Weeks and Sun (ref. 24) for composites with a variety of fiber orientations and laminate configurations at strain rates of 1×10^{-5} and 0.1/sec. Only low strain rate composite data were examined since only low strain rate data were available for the PEEK matrix.

The fiber volume fraction of the AS4/PEEK composites is 0.62. The elastic properties of the AS4 fibers were taken from reference 23 and are given in table I. The material properties of the PEEK matrix were determined using tensile stress-strain curves obtained by Bordonaro (ref. 16) over strain rates ranging from 1×10^{-6} to 1×10^{-3}/sec. The computed constants are shown in table II. Again the value for the constant "β" required for the correction factor given in equation (4) was found to be strain rate dependent. The constant "q" for this material is assumed to be rate independent. In actuality, the value of "q" was found to vary slightly with strain rate, but for the strain rates considered a constant value of "q" was acceptable. If a wider range of strain rates would be examined (like for the 977–2 resin), most likely the value of "q" for PEEK would also turn out to be rate dependent. Experimental and computed curves for the PEEK matrix are shown in figure 8. As can be seen in the figure, there is an excellent correlation between the experimental and computed curves.

Analysis Results

Experimental and computed stress-strain curves for the IM7/977–2 system are shown in figures 9 to 11. Three fiber slices were used in the analysis cell (N_f = 3) for the computations. This value was found to yield sufficiently converged answers. In figure 9, results for the [45°] laminates at strain rates of 4.75×10^{-5}/sec and 1.0/sec are shown. In figure 10, results for the [90°] laminates at 4.44×10^{-5}/ and 1.06/sec are shown. In figure 11, results for the $[\pm45°]_s$ laminates at 9×10^{-5} and 2.0/sec are shown. Note that for the [90°] laminates the experimental results show minimal rate dependence and the computed results for both strain rates overlap each other. The lack of rate dependence in the [90°] laminates is most likely due to the specimens failing while the effective stresses in the matrix were still in the elastic range. The fact that the computed results also predict a mostly linear deformation response seems to support this hypothesis. As can be seen in figure 7, all of the strain rate dependence in the matrix deformation is in the inelastic range of the stress-strain curve. As can be seen in the figures, the rate dependence (or lack thereof as in the case of the [90°] laminates) and nonlinearity of the experimental stress-strain curves are captured by the analytical model. Furthermore, the comparison between the experimental and computed results is quite good.

Experimental and computed results for the AS4/PEEK composite are shown in figures 12 to 14. Three fiber slices were again used in the analysis cell (N_f = 3) for the computations. In figure 12, results for the [45°] laminates at strain rates of 1×10^{-5} and 0.1/sec are shown. In figure 13, results for the [90°] laminates at 1×10^{-5} and 0.1/sec are shown. In figure 14, results for the $[\pm45°]_s$ laminates at 1×10^{-5} and 1.0/sec are shown. Note that for the [90°] laminates the experimental and computed results are once again strain rate independent, for the reasons discussed earlier. Another interesting point to note is that the failure strain for the [90°] laminates is relatively low. This result may be due to a low interface strength in the composite. The rate dependence and nonlinearity of the composite response are again captured by the analysis. Furthermore, the comparison between the experimental and computed results is again quite good.

To demonstrate the improvement in results obtained by using the new micromechanical formulation, figures 5 and 7 from reference 2 are reproduced in figures 15 and 16. These figures show results computed using the original micromechanics methodology, which was described in the Background section. As a reminder, in the original micromechanics method (fig. 1) the unit cell was divided into four subcells and the slicing technique was not used.

Figure 15 contains experimental and computed results for the AS4/PEEK [45°] laminates and figure 16 contains results for the AS4/PEEK $[\pm 45°]_s$ laminates described earlier. By comparing figures 15 to 12 and figures 16 to 14, using the revised micromechanics formulation results in a slight improvement in the quality of the predictions (compared to the experimental results) in the elastic range, and a significant improvement in the quality of the predictions in the inelastic range of the deformation. Furthermore, using a more refined unit cell did not significantly decrease the computational efficiency.

CONCLUSIONS

In this study, a previously developed micromechanics method has been revised in order to more accurately predict the nonlinear, strain rate dependent deformation response of polymer matrix composites composed of ductile matrix materials. In the revised micromechanics model, the unit cell is divided up into several slices, and micromechanics equations are then developed for each slice. The results from each slice are then combined using laminate theory to obtain the effective elastic properties, stresses, and inelastic strains for the unit cell. Laminate theory can be applied again to obtain the deformation response for a multilayered laminate. Tensile stress-strain curves have been computed for two representative polymer matrix composites for several laminate configurations and strain rates, and the results compared well to experimentally obtained values. Furthermore, results computed using the revised approach compared better to experimentally obtained values than results computed using the original micromechanics approach without a decrease in computational efficiency. Therefore, the revised micromechanics approach appears to be more advantageous to use.

Future efforts will include expanding the laminate theory formulations to account for unsymmetric laminates and laminates subject to bending loads. The ability to account for thermal effects will also be added to the micromechanics and laminate theory. The characterization of high strain rate tests on the IM7/977–2 system will be completed and documented. Failure theories will be added to the analytical model, and the resulting models will be incorporated within appropriate finite element codes. Furthermore, the analytical methods will be extended to the analysis of filament wound and woven composites.

REFERENCES

1. Goldberg, R.K.: “Strain Rate Dependent Deformation and Strength Modeling of a Polymer Matrix Composite Utilizing a Micromechanics Approach.” NASA/TM-1999–209768, 1999.
2. Goldberg, R.K.: “Implementation of Laminate Theory Into Strain Rate Dependent Micromechanics Analysis of Polymer Matrix Composites.” NASA/TM-2000–210351, 2000.
3. Sun, C.T.; and Chen, J.-L.: “A Micromechanical Model for Plastic Behavior of Fibrous Composites.” Composites Science and Technology, Vol. 40, pp. 115–129, 1991.
4. Robertson, D.D.; and Mall, S.: “Micromechanical Analysis for Fiber Reinforced Composites Using the Free Transverse Shear Approach.” Journal of Composites Technology and Research, Vol. 15, pp. 181–192, 1993.
5. Pecknold, D.A.; and Rahman, S.: “Application of a New Micromechanics-Based Homogenization Technique for Nonlinear Compression of Thick-Section Laminates.” Compression Response of Composite Structures, ASTM STP 1185, S.E. Groves and A.L. Highsmith, eds., ASTM, pp. 34–54, 1994.
6. Pindera, M.J.; and Bednarcyk, B.A.: “An efficient implementation of the generalized method of cells for unidirectional, multi-phased composites with complex microstructures.” Composites: Part B, Vol. 30, pp. 87–105, 1999.
7. Paley, M.; and Aboudi, J.: “Micromechanical Analysis of Composites by the Generalized Method of Cells.” Mechanics of Materials, Vol. 14, pp. 127–139, 1992.
8. Whitney, J.M.: “A Laminate Analogy for Micromechanics.” Proceedings of the American Society of Composites Eighth Technical Conference, G. Newaz, ed., Technomic Publishing Company, Lancaster, PA, pp. 785–794, 1993.
9. Greszczuk, L.B.: “Interfiber Stresses in Filamentary Composites.” AIAA Journal, Vol. 9, pp. 1274–1280, 1971.
10. Mital, S.K.; Murthy, P.L.N.; and Chamis, C.C.: “Micromechanics for Ceramic Matrix Composites Via Fiber Substructuring.” Journal of Composite Materials, Vol. 29, pp. 614–633, 1995.

11. Stouffer, D.C.; and Dame, L.T.: Inelastic Deformation of Metals. Models, Mechanical Properties and Metallurgy. John Wiley and Sons, New York, 1996.
12. Ward, I.M.: Mechanical Properties of Solid Polymers. John Wiley and Sons, New York, 1983.
13. Valisetty, R.R.; and Teply, J.L.: "Overall Instantaneous Viscoelastic Properties of Composites." Journal of Composite Materials, Vol. 26, pp. 1708–1724, 1992.
14. Zhang, C.; and Moore, I.D.: "Nonlinear Mechanical Response of High Density Polyethylene. Part II: Uniaxial Constitutive Model." Polymer Engineering and Science, Vol. 37, pp. 414–420, 1997.
15. Bodner, S.R.: "Review of a Unifed Elastic-Viscoplastic Theory." Unified Constitutive Models for Creep and Plasticity, A.K. Miller, ed., Elsevier, Barking, Essex, England, pp. 273–301, 1987.
16. Bordonaro, C.M.: "Rate Dependent Mechanical Behavior of High Strength Plastics: Experiment and Modeling." Ph.D. Dissertation, Rensselaer Polytechnic Institute, Troy, New York, 1995.
17. Krempl, E.; McMahon, J.J.; and Yao, D.: "Viscoplasticity Based on Overstress with a Differential Growth Law for the Equilibrium Stress." Mechanics of Materials, Vol. 5, pp. 35, 1986.
18. Miller, E.: Introduction to Plastics and Composites. Marcel Drekker, Inc., New York, 1996.
19. Agarwal, B.D.; and Broutman, L.J.: Analysis and Performance of Fiber Composites. John Wiley and Sons, New York, 1990.
20. Kreyszig, E.: Advanced Engineering Mathematics, 7th Edition. John Wiley and Sons, New York, 1992.
21. Goldberg, R.K.; Roberts, G.D.; and Gilat, A.: "Experimental and Analytical Studies of the High Strain Rate Tensile Response of a Polymer Matrix Composite Utilizing a Micromechanics Approach," To Be Published.
22. Gates, T.S.; Chen, J.-L.; and Sun, C.T.: "Micromechanical Characterization of Nonlinear Behavior of Advanced Polymer Matrix Composites." Composite Materials: Testing and Design (Twelfth Volume), ASTM STP 1274, R.B. Deo and C.R. Saff, eds., ASTM, pp. 295–319, 1996.
23. Murthy, P.L.N.; Ginty, C.A.; and Sanfeliz, J.G.: "Second Generation Integrated Composite Analyzer (ICAN) Computer Code." NASA TP–3290, 1993.
24. Weeks, C.A.; and Sun, C.T.: "Nonlinear Rate Dependence of Thick-Section Composite Laminates." High Strain Rate Effects on Polymer, Metal and Ceramic Matrix Composites and Other Advanced Materials, AS-Vol. 48, Y.D.S. Rajapakse and J.R. Vinson, eds., ASME, pp. 81–95, 1995.

TABLE I.—MATERIAL PROPERTIES FOR IM7 AND AS4 FIBERS

	Longitudinal modulus, GPa	Transverse modulus, GPa	Longitudinal Poisson's ratio	Transverse Poisson's ratio	In-plane shear modulus, GPa
IM7	276	12.4	0.25	0.25	20.0
AS4	214	14.0	0.20	0.25	28.0

TABLE II.—MATERIAL PROPERTIES FOR FIBERITE 977–2 (STRAIN RATES OF 5×10^{-5} AND 1/sec) AND PEEK (STRAIN RATES OF 1×10^{-5} AND 0.1/sec). FOR RATE DEPENDENT PROPERTIES, TOP CELL EQUALS VALUE AT LOWER STRAIN RATE, BOTTOM CELL EQUALS VALUE AT HIGHER STRAIN RATE

	E, GPa	ν	D_o, 1/sec	N	Z_o, MPa	Q	Ω_m, MPa	β
977–2	3.52	0.40	1E+06	0.42	2180	85	76	1.05
						160		0.90
PEEK	4.00	0.40	1E+04	0.70	630	310	52	0.40
								0.30

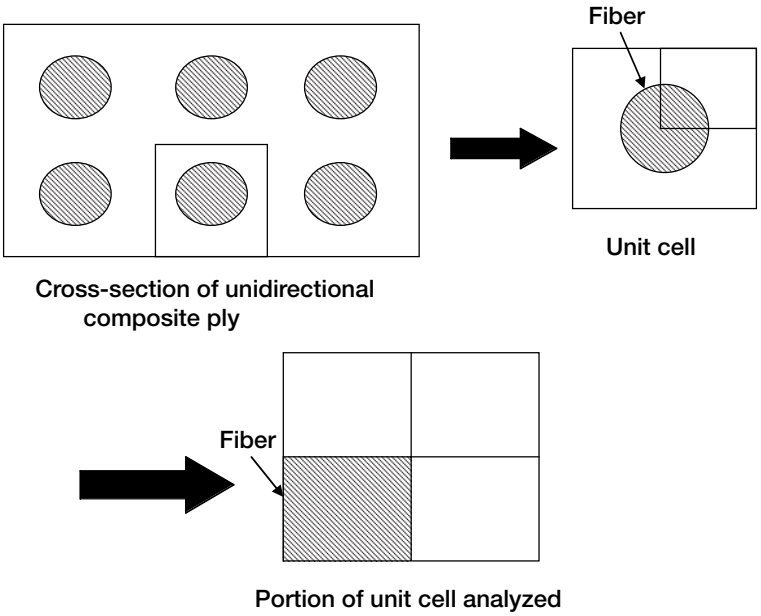

Figure 1.—Schematic showing relationship between composite ply, unit cell and portion of unit cell which is analyzed for original micromechanics model.

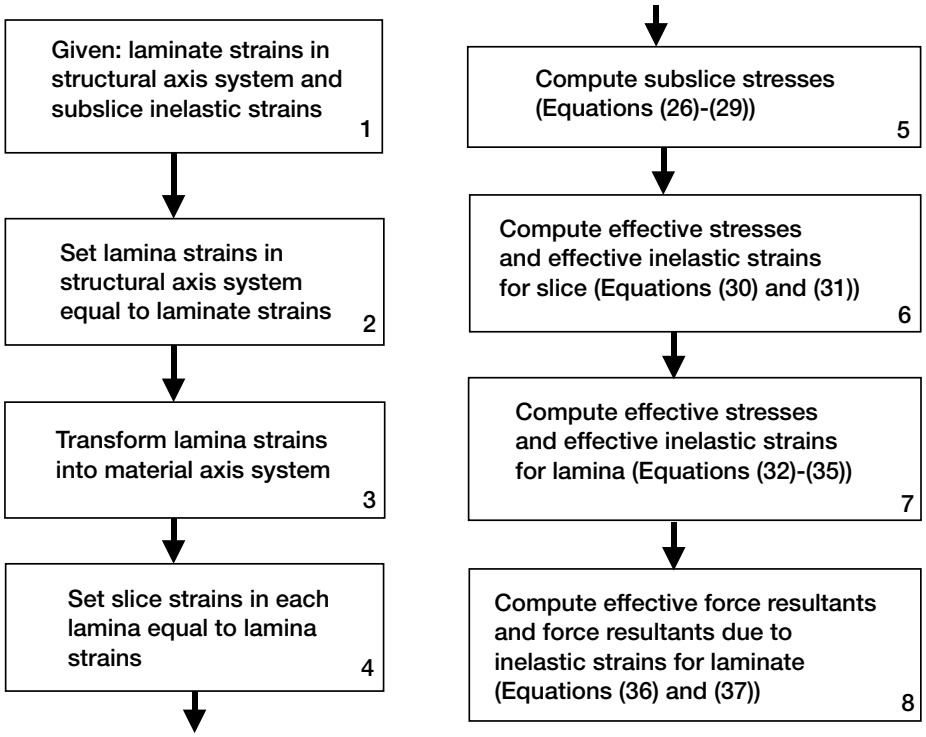

Figure 2.—Flowchart showing analysis process for revised micromechanics model.

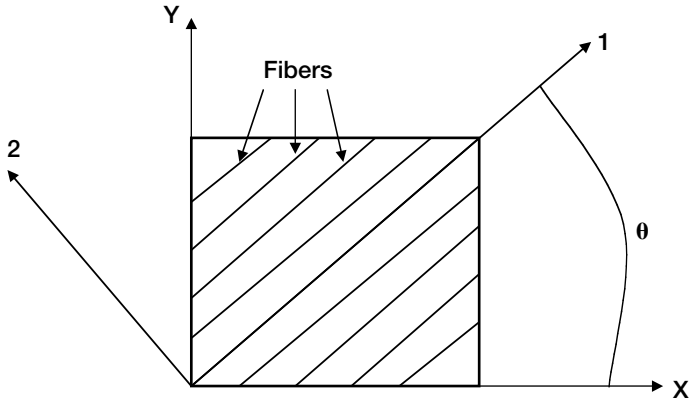

Figure 3.—Schematic showing global laminate structural axis system (X-Y axes), local material axis system (1-2 axes) and fiber orientation angle θ for a composite ply.

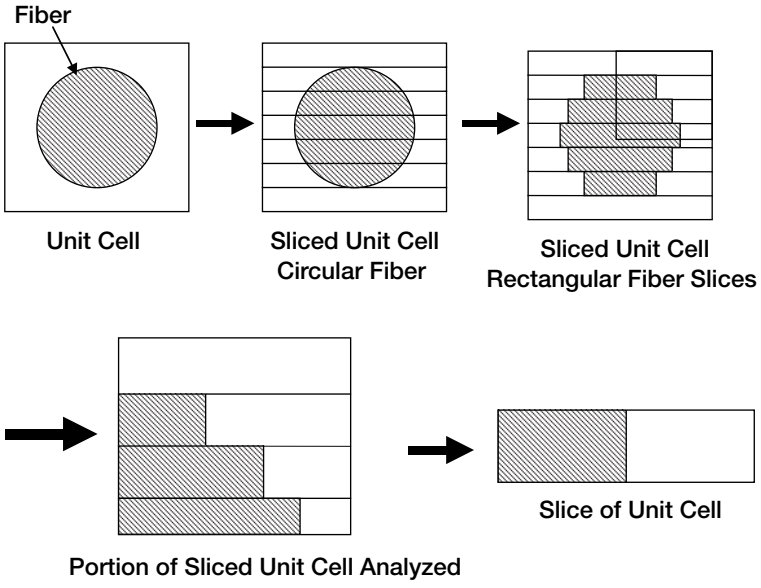

Figure 4.—Schematic showing relationship between unit cell, portion of unit cell which is analyzed and slices for revised micromechanics.

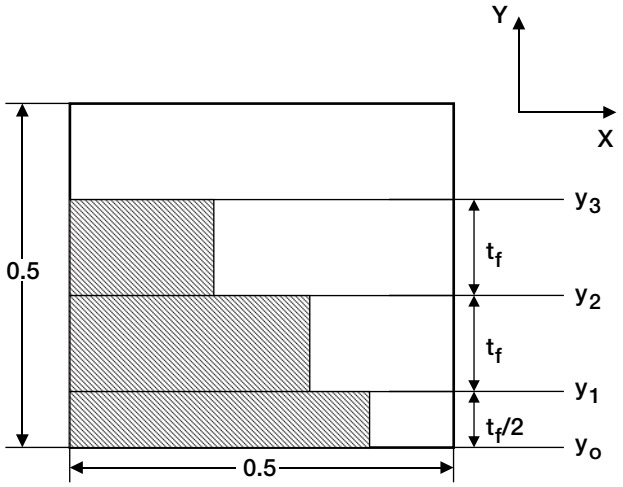

Figure 5.—Schematic showing analysis cell geometry and layout including slices for revised micromechanics model.

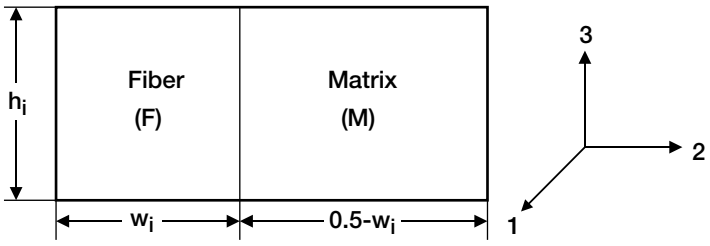

w_i = fiber subslice width
h_i = slice thickness

Figure 6.—Schematic showing slice geometry and layout for revised micromechanics model.

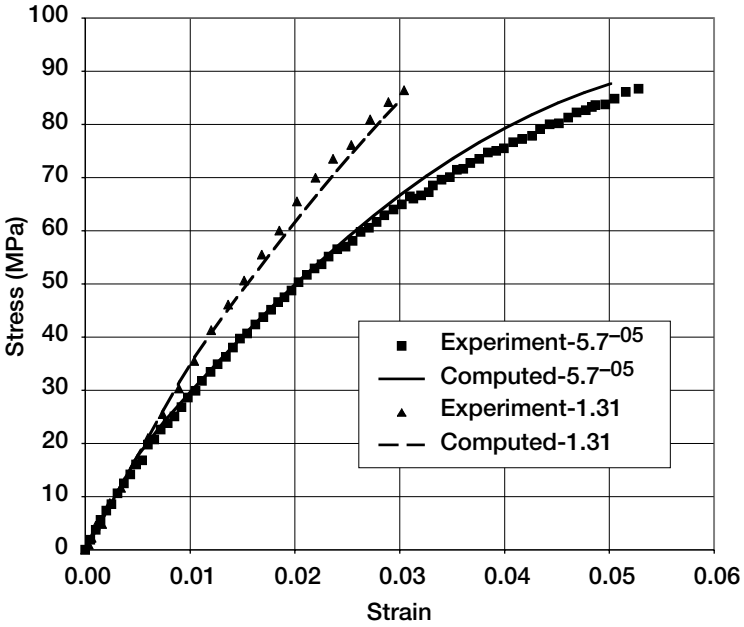

Figure 7.—Experimental and computed results for 977-2 resin at strain rates of 5.7×10^{-5}/sec and 1.31/sec.

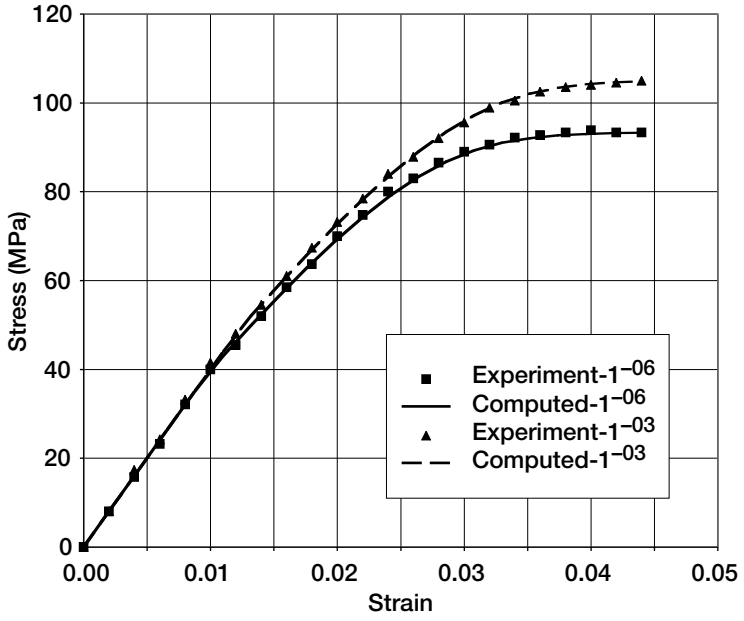

Figure 8.—Experimental and computed results for PEEK at strain rates of 1×10^{-6}/sec and 1×10^{-3}/sec.

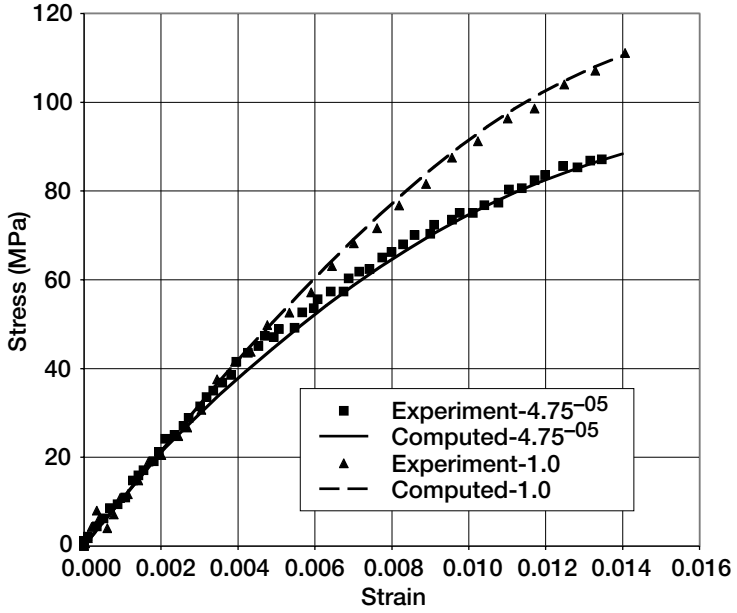

Figure 9.—Experimental and computed results for IM7/977-2 [45°] laminates at strain rates of 4.75×10^{-5}/sec and 1.0/sec.

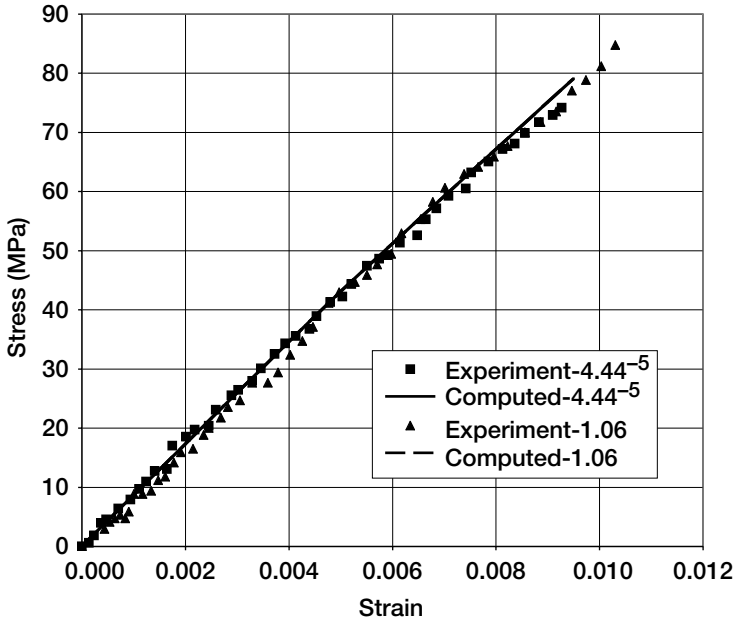

Figure 10.—Experimental and computed results for IM7/977-2 [90°] laminates at strain rates of 4.44×10^{-5}/sec and 1.06/sec.

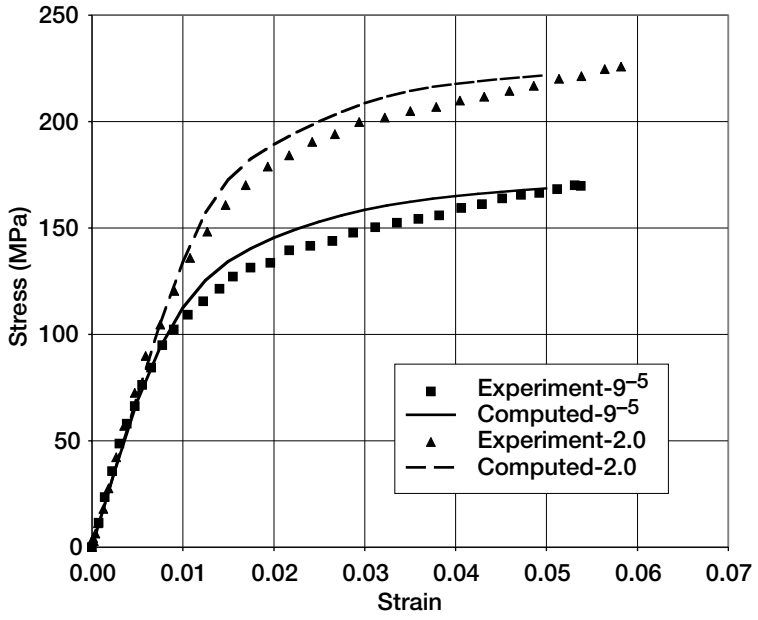

Figure 11.—Experimental and computed results for IM7/977-2 $[\pm 45^\circ]_s$ laminates at strain rates of 9×10^{-5}/sec and 2.0/sec.

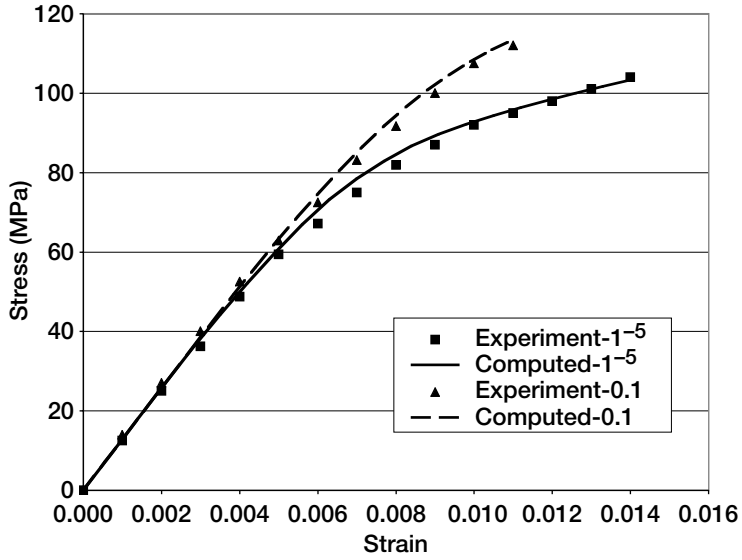

Figure 12.—Experimental and computed results for AS4/PEEK [45°] laminates at strain rates of 1×10^{-5}/sec and 0.1/sec.

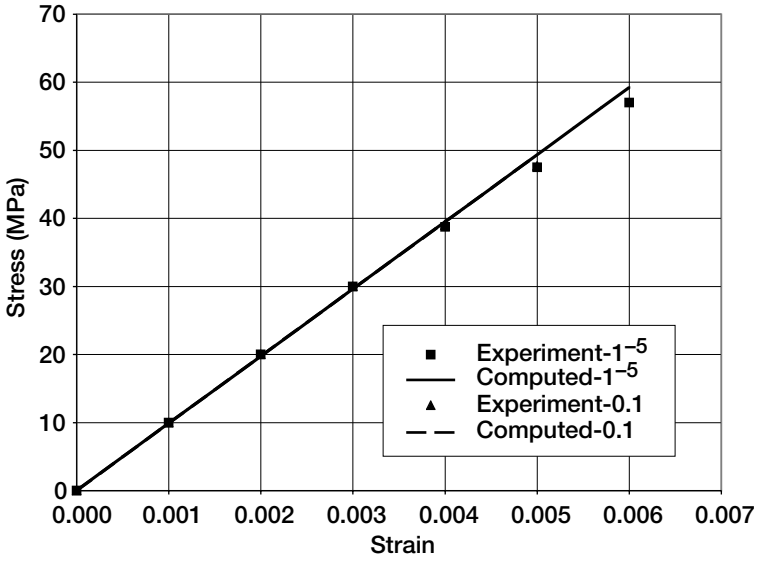

Figure 13.—Experimental and computed results for AS4/PEEK [90°] laminates at strain rates of $1x10^{-5}$/sec and 0.1/sec.

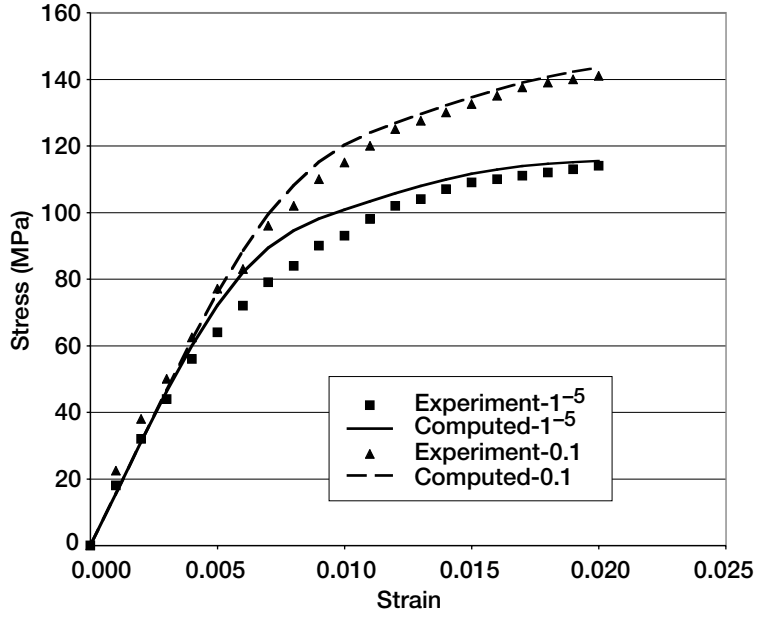

Figure 14.—Experimental and computed results for AS4/PEEK $[\pm 45^\circ]_s$ laminates at strain rates of $1x10^{-5}$/sec and 0.1/sec.

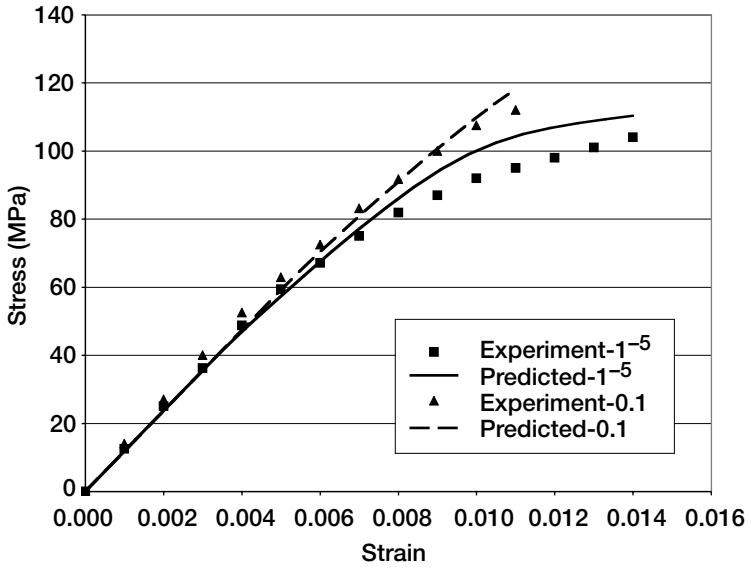

Figure 15.—Experimental values for AS4/PEEK [45°] laminates at strain rates of $1x10^{-5}$/sec and 0.1/sec and results computed using original micromechanics model.

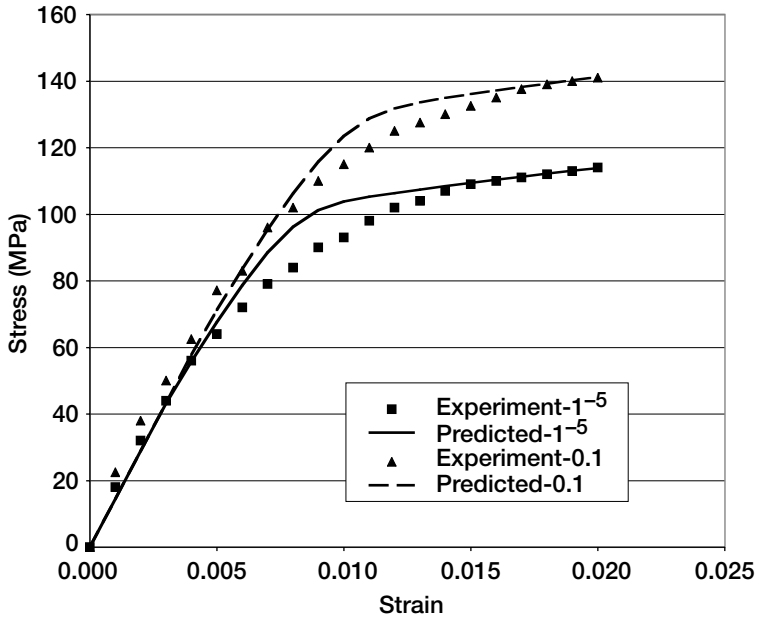

Figure 16.—Experimental values for AS4/PEEK $[\pm 45°]_s$ laminates at strain rates of $1x10^{-5}$/sec and 0.1/sec and results computed using original micromechanics model.

REPORT DOCUMENTATION PAGE

Form Approved
OMB No. 0704-0188

1. AGENCY USE ONLY (*Leave blank*)	2. REPORT DATE	3. REPORT TYPE AND DATES COVERED
	April 2001	Technical Memorandum

4. TITLE AND SUBTITLE

Implementation of Fiber Substructuring Into Strain Rate Dependent Micromechanics Analysis of Polymer Matrix Composites

5. FUNDING NUMBERS

WU–708–24–13–00

6. AUTHOR(S)

Robert K. Goldberg

7. PERFORMING ORGANIZATION NAME(S) AND ADDRESS(ES)

National Aeronautics and Space Administration
John H. Glenn Research Center at Lewis Field
Cleveland, Ohio 44135–3191

8. PERFORMING ORGANIZATION REPORT NUMBER

E–12740

9. SPONSORING/MONITORING AGENCY NAME(S) AND ADDRESS(ES)

National Aeronautics and Space Administration
Washington, DC 20546–0001

10. SPONSORING/MONITORING AGENCY REPORT NUMBER

NASA TM—2001-210822

11. SUPPLEMENTARY NOTES

Responsible person, Robert K. Goldberg, organization code 5920, 216–433–3330.

12a. DISTRIBUTION/AVAILABILITY STATEMENT

Unclassified - Unlimited
Subject Category: 24 Distribution: Nonstandard

Available electronically at http://gltrs.grc.nasa.gov/GLTRS

This publication is available from the NASA Center for AeroSpace Information, 301–621–0390.

12b. DISTRIBUTION CODE

13. ABSTRACT ***(Maximum 200 words)***

A research program is in progress to develop strain rate dependent deformation and failure models for the analysis of polymer matrix composites subject to impact loads. Previously, strain rate dependent inelastic constitutive equations developed to model the polymer matrix were incorporated into a mechanics of materials based micromechanics method. In the current work, the micromechanics method is revised such that the composite unit cell is divided into a number of slices. Micromechanics equations are then developed for each slice, with laminate theory applied to determine the elastic properties, effective stresses and effective inelastic strains for the unit cell. Verification studies are conducted using two representative polymer matrix composites with a nonlinear, strain rate dependent deformation response. The computed results compare well to experimentally obtained values.

14. SUBJECT TERMS

Composite materials; Impact; Micromechanics; Viscoplasticity; Strain rate

15. NUMBER OF PAGES

31

16. PRICE CODE

A03

17. SECURITY CLASSIFICATION OF REPORT	18. SECURITY CLASSIFICATION OF THIS PAGE	19. SECURITY CLASSIFICATION OF ABSTRACT	20. LIMITATION OF ABSTRACT
Unclassified	Unclassified	Unclassified	